Catalysis Today 180 (2012) 174–183

Contents lists available at ScienceDirect

Catalysis Today

journal homepage: www.elsevier.com/locate/cattod

A novel procedure for accurate estimations of the lattice parameter of supported nanoparticles from the analysis of plan view HREM images: Application to the structural investigation of Pd/CeO_2 catalysts

C. Mira*, J.J. Calvino, J.A. Pérez-Omil, J.M. Rodríguez-Izquierdo, S. Bernal

Departamento de Ciencia de los Materiales e Ingeniería Metalúrgica y Química Inorgánica, Facultad de Ciencias, Universidad de Cádiz, Campus Rio San Pedro s/n, Puerto Real, 11510 Cádiz, Spain

ARTICLE INFO

Article history:
Received 8 March 2011
Accepted 13 April 2011
Available online 12 July 2011

Keywords:
Lattice parameter measurements
HREM
Pd/CeO_2 catalyst
Metal-support interaction

ABSTRACT

A new procedure to determine, with very high accuracy, the lattice parameter of individual supported nanoparticles of interest in catalytic system is presented, checked and applied to ceria supported Palladium catalysts. The procedure is based on the analysis of double diffraction effects present in High Resolution Electron Microscopy (HREM) images recorded in top view conditions. For nanoparticles about 5 nm in diameter accuracies in the order of ±0.2% are demonstrated by using a method in which intensity profiles of Digital Diffraction Patterns obtained from experimental HREM images are fitted to a set of Lorentzian-type functions. The new method allows characterizing the distribution of lattice parameter of nanoparticles in systems which are out of range for XRD, as it is the case of catalysts with very low loadings or those in which the particle size distribution is dominated by very small (<5 nm) nanoparticles. In the Pd/CeO_2 catalysts investigated, evidences of phenomena of large interest to understand the catalytic behaviour like Pd–Ce alloying or Pd nanoparticle encapsulation have been evidenced by measurements of Pd lattice parameters performed using the new method on catalyst reduced at high temperatures (>773 K). Likewise, in Pd/CeO_2 catalysts reduced at low temperatures (<773 K), structural accommodation phenomena of the metal nanoparticles on the ceria support have been revealed whose intensity depends both on the particle diameter and on reduction temperature.

1. Introduction

Ceria and ceria-supported metal catalysts have been applied for many years as components of Three-Way Catalysts (TWC) [1]. Several roles have been attributed to ceria and ceria-based mixed oxides in this application, namely oxygen storage and release under fuel-lean and fuel-rich conditions respectively, a promotional effect of water gas shift reaction or the stabilization of the metal dispersion [2]. Later, CeO_2–ZrO_2 mixed oxides substituted pure ceria in this application due to their improved textural stability and higher oxygen storage capacity. Platinum group metals (Pd, Pt, Rh) have been those usually employed as active metal components in TWCs [3]. Due both to socioeconomic aspects and to its high efficiency in oxidation reactions, considerable attention has also been paid to the use of Pd-only TWCs.

Automotive exhaust catalysts are usually exposed for long periods to harsh working conditions, especially in terms of temperature, which occasionally can reach values higher than 1100 °C [4]. The combination of such high temperature conditions with the reducing environment which prevails during the oxygen lean excursions of the working cycle may promote the interaction between metal and ceria, and eventually lead to a modification of the catalyst activity linked to phenomena like: decoration of the surface of the metal nanoparticles by support patches, as it has been previously observed in Rh/CeO_2 [5] and Pt/CeO_2 [6] catalysts; encapsulation of the metal nanoparticles by support material as proposed for $Pd/CeZrO_2$ catalysts [7] from the analysis of Pd-peak positions in X-ray diffraction patterns, and which results in an irreversible loss of metal active sites; formation of Metal–Ce alloys or intermetallic compounds as reported for Pt [6] and Pd [8].

However, changes in the nanostructure of these catalysts can also be related to modifications in the lattice parameter of the metal nanoparticles with respect to bulk Pd. It becomes clear that such deviations involve modifications in the electronic properties of the metal particles which can eventually also influence to some extent their catalytic performance.

Expansion or contraction of the lattice constant of supported metal nanoparticles have been related to a number of effects: incorporation of support elements into the particles in the form of alloys

* Corresponding author. Tel.: +34 647584883; fax: +34 956016288.
E-mail address: cesar.mira@uca.es (C. Mira).

0920-5861/$ – see front matter © 2011 Elsevier B.V. All rights reserved.
doi:10.1016/j.cattod.2011.04.034

[8,9]; incorporation of small atoms of other elements, like H, O, or C, into the metal lattice [10]; pseudomorphic growth (perfect accommodation between the particles and substrate lattices) [11,12] and surface stress or encapsulation of the metal under a large compressive stress by the substrate [7,13]. The observed modifications of the lattice parameter are frequently smaller than 5%. Therefore, in order to draw meaningful conclusions from these very subtle nano-structural effects, measurements of the lattice spacing values with accuracy better than 1% are required [9]. A precise quantification of metal lattice parameter modifications can in any case help to elucidate their precise origin. Accurate determination of lattice spacing values in nanosized crystallites and their modification with particle size is a question of great interest due to its eventual relationship with their electronic and chemical properties.

Different techniques have been proposed to determine changes in lattice spacing values, X-ray diffraction being possibly the most widely used. Despite its high accuracy, this technique provides only an average value for the material under study. Likewise, it can hardly be reliably used in those cases in which broad peaks with low signal to noise ratio, often found in supported metal catalysts, have to be analyzed. XAFS can also be used to estimate these changes [14]. Likewise, lattice parameters have been measured in situ by surface electron energy-loss fine-structure spectroscopy (SEELFS) [12] with a precision close to 1%. However, these techniques, as XRD, only allow a macroscopic approach and provide only average values for the whole set of nanoparticles present in the sample.

In a more localized approach, Selected Area Diffraction Patterns (SAED) can be used to determine lattice parameters on regions containing particles of uniform size and composition. Nevertheless, SAED patterns allow only estimations with high relative errors (2–3%). The use of higher-order terms in the classic Bragg law approach relating lattice spacing values to distances measured on electron diffraction patterns and an internal reference may improve the accuracy. By analysing all the diffraction rings, in effect, the lattice parameter of a polycrystalline sample may be determined with a precision better than 0.05% [15]. In this approach, the diffraction peaks were fit to Lorentzian functions which provided the location of the peak centres and the standard deviations of every fit.

Finally, measurements on High Resolution Electron Microscopy images would allow the most localized type of analysis, by studying single particles. However, as with SAED patterns, the accuracy of direct measurements on HREM images of nanosized particles is not better than 5% [16].

A statistical approach can improve the accuracy of HREM measurements when a large number of particles are simultaneously studied [8,9,15], but in this case we are not characterising a single particle but an ensemble.

Lattice spacing measured from HREM images of small particles can deviate from the expected value in some cases up to a 10% [16]. This type of measurement is highly sensitive to the tilt of the nanoparticle with respect to the electron beam. Moreover, apparent "surface relaxation" effects, due to Fresnel diffraction effects at surfaces, also show up in the diffractograms of experimental HREM images and can result in deviations with respect to the exact lattice spacing up to 15% [16]. This apparent relaxation of the surface layer is an inherent artefact of the diffractogram approach to determine lattice spacing [16]. The viewing direction has to be accurately determined; otherwise the measured values might not give reliable information about the actual structure of the particle. In fact, the accuracy with this measurement technique depends on several experimental factors like the calibration method, the specimen characteristics, the total electron dose, the image detection system or the size of measurement area [17]. To measure lattice parameters of a collection of nanoparticles by HREM, a reference material is required for calibration.

To increase the accuracy in the determination of lattice spacing values of nanoparticles, statistical methods have been proposed [9,17]. In this case, the average lattice spacing of an ensemble of nanoparticles is obtained. The approach usually involves calculating the Fast Fourier Transform (FFT) of a region of the image comprising a set of particles. Then a digital diffractogram is generated by representing for example a version of the log scaled power spectrum of the FFT. In this diffractogram, also usually referred to as DDP (digital diffraction pattern) each set of lattice planes is related to one spot. The fringe spacing is then measured using interpolation routines to determine, with sub-pixel accuracy, the centre of the corresponding reflection in the DDP. The accuracy of the lattice measurement on an individual particle is limited by an effective standard deviation which depends on the size of the individual nanoparticle. By measuring roughly 100 nanoparticles with sizes in the range of 2–3 nm, the average lattice spacing can be determined with accuracy close to 0.2%.

In the present study a new procedure to improve accuracy in measurement of lattice parameter has been developed based on the analysis of HREM images of individual supported nanoparticles recorded in plan view conditions. The method has been used to investigate the structural modifications occurring in Pd nanoparticles supported on a cerium dioxide upon activation in hydrogen at increasing temperatures.

As deduced from the whole set of results reported herein, this new method may fruitfully be used to gain rather fine nanostructural information about the nature of metal-support interaction effects occurring in Pd/ceria catalysts as a function of the applied reduction pretreatment.

2. Experimental

The two Pd/CeO_2 catalysts studied in this work were prepared by impregnation of a ceria powder with an aqueous solution of Pd nitrate to incipient wetness, followed by drying at 393 K for ten hours and further calcination at 823 K for two hours. The following Pd loadings were determined by ICP: 0.5 and 2.4 wt% Pd. The ceria powders used as support, with 20 m^2/g surface area, were supplied by Rhodia. Catalysts were finally reduced in flow of H_2(5%)/Ar at 473 K, 623 K, 773 K, 973 K and 1173 K for one hour, followed by evacuation in He flow at the same temperature for 1 h. In the case of 473 K and 623 K reductions the evacuation temperature was 773 K. After reduction and evacuation the samples were submitted to a passivation treatment to avoid uncontrolled reoxidation of the ceria support when exposed to air which could irreversibly modify the structure of the catalysts. This passivation treatment was performed as reported previously for other metal/ceria catalysts [5], by flowing a mixture of O_2 (5%)/He over the catalysts from 178 K up to room temperature. Catalysts were characterized by XRD and HREM.

XRD diffraction data were obtained with a Philips PW 1820 powder diffractometer using Cu Kα radiation. The intensities were recorded in the 2θ range from 20° to 110° with a step of 0.05° and a measuring time of 60 s at each point. This high time per step value has allowed us carrying out a Rietveld refinement of the diffraction diagrams. This procedure provides not only the percentage and average crystallite size of each phase present in the sample, but also determines the value of the lattice parameters of each structure contributing to the diagram.

HREM studies were performed with a JEOL 2000 EX microscope equipped with a top-entry sample holder and operating at 200 kV. The structural resolution of this microscope was 0.21 nm. Samples were supported on a copper grid covered with a holey carbon film. Digital analysis of the images was carried out with SEMPER 6+ software.

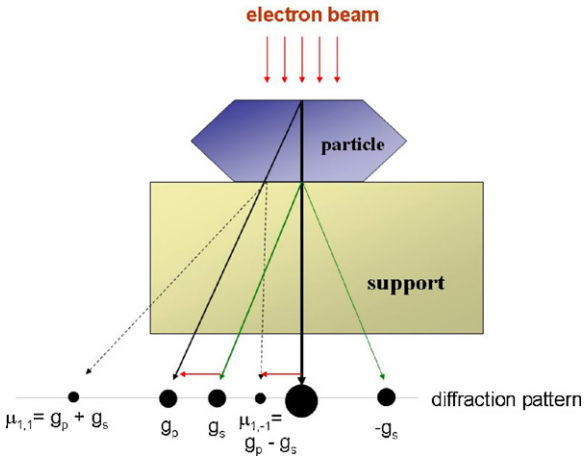

Fig. 1. Sketch explaining the origin of the Moiré reflections by double diffraction in a supported nanoparticle system (g_p and g_s correspond to the diffracted beams of the particle and the support respectively).

HREM simulation images were obtained using the EMS software running on an Indy 4400SC Silicon Graphics Workstation. The structural models were built using the RHODIUS software [18].

3. Results and discussion

3.1. A novel approach to estimate lattice parameter of nanoparticles from top view HREM images

We will begin this section providing some details about a new procedure developed to increase the accuracy in the determination of the lattice spacing values of individual supported nanoparticles from the detailed analysis of their top view HREM images. The procedure relies on the quantification of double diffraction effects. This double diffraction phenomenon takes place as follows (see sketch in Fig. 1): when the incident electron beam impinges on the supported nanoparticle a first diffraction event takes place which gives rises in addition to the incident beam to a series of diffracted beams. Since the interaction of electrons with matter is quite strong (hundreds of times more intense than with X-rays), the intensity of the diffracted beams when they exit the particles is usually very high. Such high intensity electron beams do behave as additional incident electron beams and, therefore, can be diffracted further by the support crystallite. This gives rise to a series of new diffracted beams which are neither those characteristic of the particle nor those of the support but, instead, as shown in Fig. 1 (dashed lines), linear combinations of them. These extra beams due to double diffraction can be detected at the diffraction stage, therefore they are observed in electron diffraction pattern. Likewise they give rise to additional fringes in HREM images, which are usually called Moiré fringes. Thus, DDPs on images containing these Moiré fringes show also extra spots related to double diffraction. As previously mentioned, these Moiré spots correspond to linear combinations (additions and differences) between the characteristic nanoparticle and support reflections. In the following we will refer to these reflections as $\mu_{x,y}$ reflections, to denote that, Eq. (1), they correspond to the combination of y times a reflection of the support (g_s) and x times a reflection of the supported particle (g_p), where both x and y can be either positive or negative numbers.

$$\mu_{x,y} = xg_p + yg_s \quad (1)$$

As it will be shown below, particles of only a few nanometers can give rise to a large number of these Moiré reflections which can be fruitfully detected in the corresponding image diffractograms. Using the lattice fringes of the bulk support as a reference, the measurement of each Moiré reflection in reciprocal space allows an estimation of the supported particle lattice spacing values.

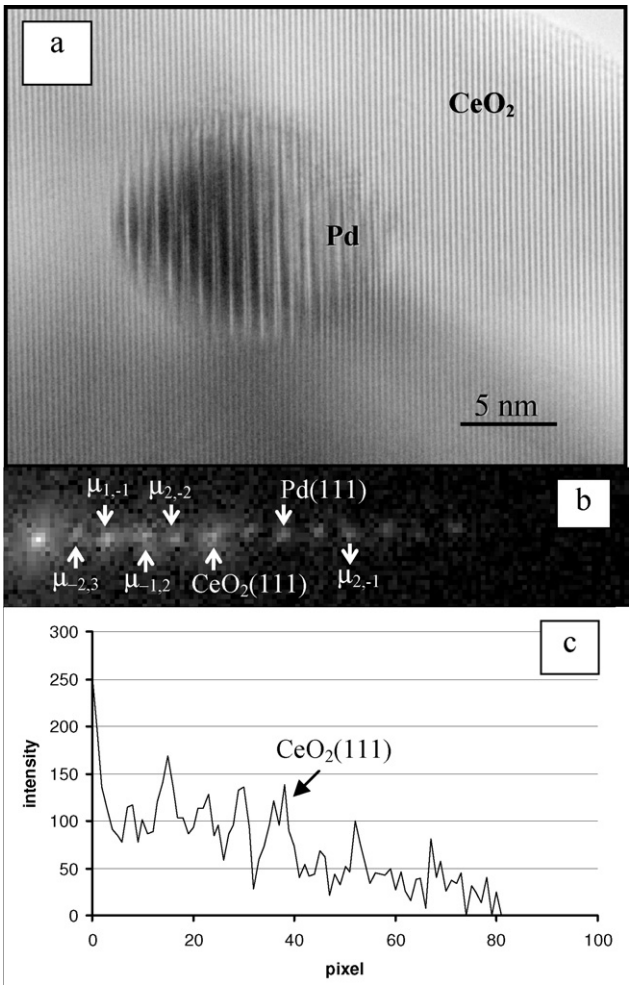

Fig. 2. (a) HREM image corresponding to a Pd(0.5%)/CeO_2 catalyst reduced at 1173 K. (b) Detail of the DDP obtained from the Pd particle. (c) Intensity Profile from the DDP.

Fig. 2 shows a top view HREM image of a CeO_2-supported Pd particle, Fig. 2(a), and its corresponding diffractogram, Fig. 2(b). The Moiré type lattice fringes are those which give rise to the low frequency details in the image of Fig. 2(a). If the DDP, Fig. 2(b) is analysed, in addition to the (1 1 1) reflections of both Palladium and ceria the following Moiré reflections can also be identified: $\mu_{-2,3}$, $\mu_{1,-1}$, $\mu_{-1,2}$, $\mu_{2,-2}$, $\mu_{2,-1}$. Note how, although the inspection of the image clearly reveals the occurrence of the double diffraction process, by the appearance of the low frequency details, the quantitative analysis of these effects can only be done on the basis of reciprocal space information, from which the contribution of all the different linear combinations can be estimated.

Intensity profiles along the direction onto which the different reflections align in the DDP can be extracted, Fig. 2(c). The maxima observed in these profiles allow precisely locating the position of the different reflections in the DDP. This information can then be analysed in different ways to extract information on the nanoparticle lattice parameters. In any case, the DDP must be taken from an area large enough to include regions of the surrounding support which are free from any supported particle. These nanoparticle-free surroundings have in fact to include areas of the support located a few nanometers away from the particle, which are those expected not to be structurally influenced by its presence on the surface. Only under these conditions it seems reasonable to use the bulk value of the support lattice plane spacing value ($g_{s0}{}^{-1}$) as internal

Table 1
Formulae of error propagation.

Function	Variance
$q = x + y$	$\delta q = \delta x + \delta y$
$q = Ax$ (A = constant)	$\delta q = A\delta x$
$q = xy$	$\delta q/q = \delta x/x + \delta y/y$
$q = x^{-1}$	$\delta q = \delta x/x^2$

calibration. With this reference, and once the position of the different maxima are measured in pixel units, the lattice spacing of the nanoparticle ($g_{p0}{}^{-1}$) can be determined either directly from its maxima, Eq. (2), or from those of the different Moirés observed in the profile, Eq. (3), according to the following expressions:

$$g_{p0} = g_p g_{s0} g_s^{-1} \quad (2)$$

$$g_{p0} = g_{s0} x^{-1} (y - \mu_{x,y} g_s^{-1}) \quad (3)$$

where g_p, g_s and $\mu_{x,y}$ are the positions on the profile, in pixel units, of the nanoparticle, the support and the Moiré (x,y) reflection maxima respectively; and g_{s0} and g_{p0} the reciprocal spacing values (in nm or Å) of the lattice planes of the nanoparticle and the support. The value $g_{p0}{}^{-1}$ would give the lattice spacing of the planes of the nanoparticle observed in the DDP.

The uncertainty in the g_{p0} value obtained as a result of the calculations performed with any of the reflections can be estimated using the formulae of error propagation included in Table 1, where δq, δx and δy are the absolute errors of q, x and y respectively.

Applying these expressions and assuming that the position of the maxima in the profiles can be determined with an accuracy of ±1 pixel, we can conclude that all the estimations performed from Moiré reflection are more precise than that made from the direct measurement of the nanoparticle reflections. The exact value of the error depends on the particular Moiré selected. To illustrate this idea, Table 2 gathers the errors in the estimation of Pd lattice parameter expected from measurements of both Pd(1 1 1) and different Moiré reflections. These estimations are based in Fig. 2(b) (119 pixels/Å^{-1}). Different metal-support orientation relationships, which involve perfect alignment between Pd and CeO_2, are considered to provide a wider perspective.

Note how, according to Table 2, the accuracy obtained from the measurement of any Moiré reflection is higher than that obtained from the metal reflection. Accuracies even fourfold higher are pos-

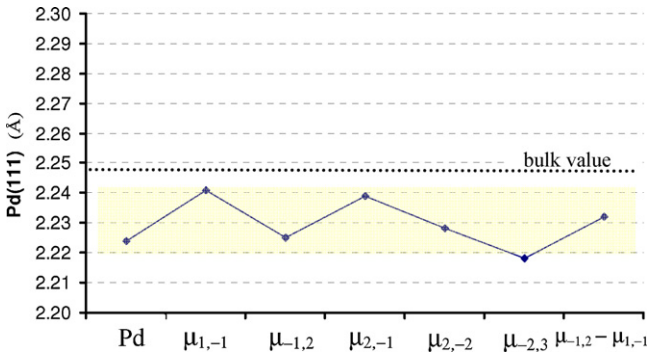

Fig. 3. Pd(1 1 1) spacing values obtained from the reflections in the DDP of Fig. 2. Bulk value is showed.

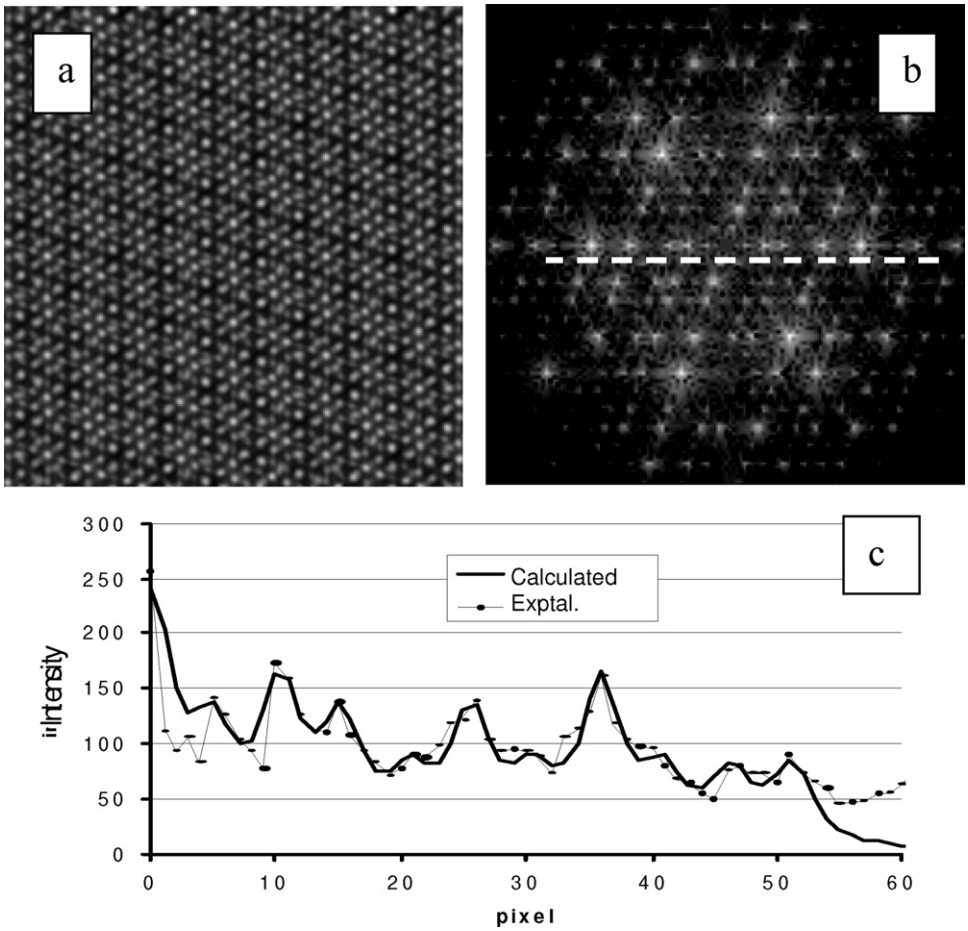

Fig. 4. (a) Simulated HREM image of a Pd layer on top of a Ceria crystallite. The Pd layer is contracted 1%. (b) DDP from (a). (c) Intensity profile from the DDP along the white dashed line.

Table 2
Estimated errors in the measurement of Pd lattice parameter using different reflections in the DDP of HREM images.

Reflection	Pd(0 0 2)|| CeO_2(0 0 2)	Pd(1 1 1)|| CeO_2(0 0 2)	Pd(1 1 1)|| CeO_2(1 1 1)
Pd	3.9%	4.2%	4.5%
$\mu_{1,-1}$	2.2%	2.2%	2.6%
$\mu_{-1,2}$	2.6%	3.4%	3.0%
$\mu_{2,-1}$	2.3%	2.3%	2.6%
$\mu_{2,-2}$	1.5%	1.3%	1.7%
$\mu_{-2,3}$	1.0%	1.5%	1.1%
$\mu_d = \mu_{-1,2} - \mu_{1,-1}$	1.8%	2.4%	2.1%

sible using some Moiré reflections. The exact Moiré which provides the best accuracy depends both on the reflections which are aligned in the DDP and the exact orientation relationship between the metal and the support.

When particles are only 1–3 nm in size the only Moiré reflections usually observed in the DDP are the $\mu_{-1,2}$ and the $\mu_{1,-1}$. Note that the accuracy corresponding to these Moirés (2.6 and 2.2%) is twofold better than the one obtainable using the metal reflection (3.9%). Moreover, the use of the difference between these two Moirés, $\mu_{-1,2} - \mu_{1,-1}$, which we have labelled as difference Moiré (μ_d) provides in general a slightly improved accuracy with respect to the use of any of the single Moirés (last line in Table 2). We should also highlight that making calculations as those presented in Table 2 allow us predicting the best approach to perform experimental measurements.

It is worth emphasizing at this point that each Moiré reflection allows calculating a statistically distinct value of the metal lattice parameter, so we can improve the accuracy in our estimation by using an average of all these values. Fig. 3, plots the values of Pd(1 1 1) spacing values determined from the analysis of the different Moiré reflections observed in Fig. 2. The plot also includes the estimations from the direct measurement of Pd(1 1 1) reflection and that corresponding to the difference between two Moirés ($\mu_{-1,2} - \mu_{1,-1}$). Note that in this case all the values are slightly smaller than that corresponding to the bulk metal (dotted reference line in the plot).

The error associated to the average is only 0.5%, a value three times smaller than that obtained by the use of a single Moiré and more than five times smaller than that characteristic of the direct Pd(1 1 1) measurement.

It becomes clear from these considerations that Moiré based approaches provide much more accurate values than those obtained by direct measurements on the metal spots. The accuracy is highly improved by averaging all the double diffraction information contained in the DDP. We can conclude at this point that these double diffraction phenomena, far from being a complication in the interpretation of HREM images, constitute, instead, a quite rich source of information. In fact, an estimation much better than the one mentioned above can be obtained if all the information present in the DDP is used simultaneously. We can perform this analysis following the procedure outlined below.

Thus, if we record an intensity profile of the DDP we can try to fit it to a theoretical curve in which the metal lattice spacing is the parameter to be refined. This fitting step would start by providing a first estimate of the position in the DDP of the support reflection (g_s), from its measurement on the experimental DDP, as well as the bulk support and metal lattice spacing values. From these figures, the position expected for the set of Moiré reflections which would lie within the reciprocal space range recorded in the DDP can be calculated. Then a set of Lorentzian type functions can be used, centred at the calculated position of the Moirés, to fit the experimental curve. The obtained fit parameters would provide the width and amplitude of each Lorentzian as well as a goodness of fit feature.

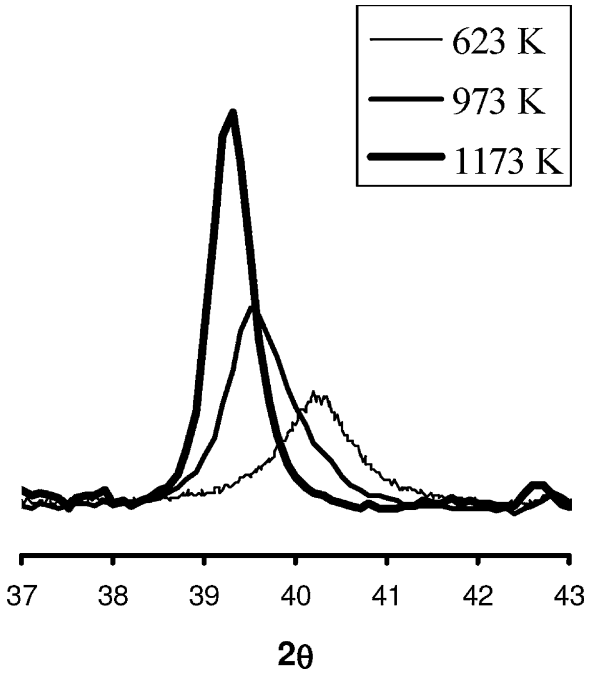

Fig. 5. Detail of XRD spectra (plane (1 1 1) of Pd) of the Pd(2.4 wt%)/CeO_2 catalyst reduced at 623 K, 973 K and 1173 K in H_2/Ar flow.

Then we can modify, within a small variation range (e.g. ±5%), the value of the metal lattice spacing. Since the positions of the Moiré reflections are quite sensitive to subtle modifications in the metal lattice parameter, the fitted curve modifies and consequently the goodness of fit value. Once the value of the particle lattice spacing providing the best fitting curve is identified, further improvement of the fitting can be tried by very slightly changing the position of the support reflection. After several iterations of this process the position, in pixel units, of the support (g_s) and of the particle (g_p) reflections providing the best fit between the experimental and calculated curves can be determined. Then, using Eq. (1), the lattice spacing of the metal (g_{p0}) can be estimated. We have developed in our lab the software to apply this approach. This program allows fitting simultaneously all the visible peaks in the intensity profile, which includes not only the metal and support peaks but also a set of Moiré reflections. The correlation coefficient between the theoretical and experimental curves shows a maximum for a precise metal spacing value, usually corresponding to situations of slight lattice contractions or expansions.

In order to estimate the confidence and expected error of the method, the approach was checked by applying it to simulated HREM images of a series of ceria-supported Pd models in which different known metal lattice expansions/contractions were considered. Fig. 4(a) shows one of these simulated images, in particular that corresponding to a 1% contracted Pd nanoparticle (5 nm thickness) supported on a ceria (5 nm thickness) support. Both CeO_2 and Pd are imaged down the [1–10] zone axis and the orientation relationship between the two components is the following: Pd(1 1 1)||CeO_2(1 1 1).

Using the program, the intensity profile of the DDP taken along the ⟨1 −1 1⟩ reciprocal direction (marked on the DDP), Fig. 4(b), was fitted, Fig. 4(c), and provided a Pd lattice parameter corresponding to a 1.0% contraction, as exactly considered in the model. Additional comparisons were also made for other contraction and expansion situations as well as for the exact bulk lattice parameter values. The Pd(1 1 1) lattice spacing estimated by our approach showed in all cases relative errors lower than 0.2%, which can be considered the error limit for this approach for particles with size about

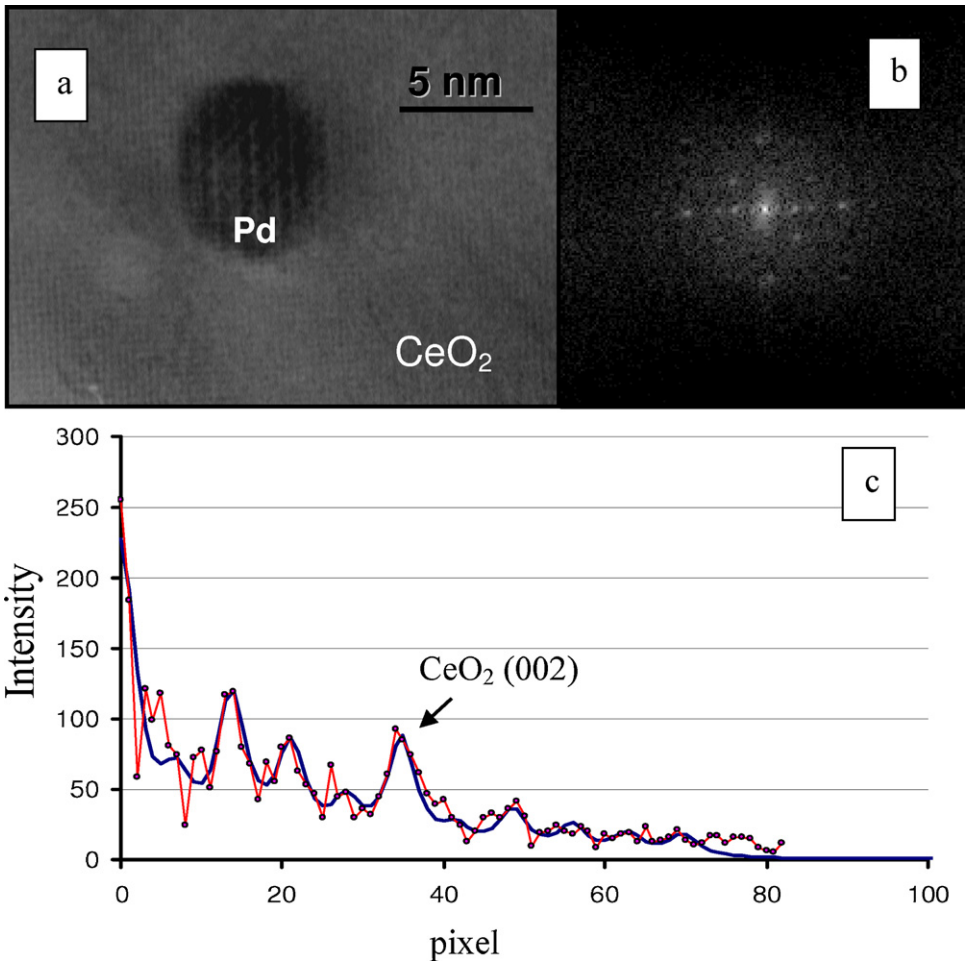

Fig. 6. (a) HREM image corresponding to the Pd(2.4 wt%)/CeO_2 sample reduced at 973 K; (b) DDP from the Pd nanoparticle; (c) intensity profile from the DDP in (b).

5 nm. For smaller particles 2–5 nm, the number of Moiré reflections appearing in the DDP decreases and this increases slightly the total error but in any case it is one order of magnitude smaller than that obtained using direct measurements of the metal reflections and about half the value characteristic for estimations based on single Moiré measurements.

We have used this experimental approach to analyse the influence of reduction treatments in flowing hydrogen at increasing temperatures (623–1123 K range) on the lattice parameter of Pd nanoparticles in Pd/CeO_2 catalysts. The consideration of the whole set of results will allow us to appreciate the complementarity of HREM to XRD as a tool to analyse the lattice parameter of nanoparticles when our method is used.

3.2. Application to Pd/CeO_2 catalysts reduced at high temperature

Fig. 5 shows the XRD diagram of the Pd(2.4 wt%)/CeO_2 catalyst, in the 2Θ range corresponding to the metallic Pd(1 1 1) peak, after reduction at 623 K, 973 K and 1173 K. A progressive shift of the Pd(1 1 1) peak to lower 2Θ values and a decrease in the peak width is clearly observed. This has been previously attributed to the incorporation of cerium into Pd and formation of Ce–Pd alloys promoted by the reduction of the support [8]. No evidence about the formation of an intermetallic phase was found. Likewise, no change in the position of the support peaks was observed. The expansion of the f.c.c. lattice of Pd associated to this alloying process as estimated from the displacement of the XRD peak was 1.6% for the catalyst reduced at 973 K (fcc, a = 0.395 nm) and 2.1% after reduction at 1173 K (fcc, a = 0.397 nm). These expansions would correspond to alloys containing about 7–8% Ce and 9–10% respectively [19]. These values are lower than those required to form the $CePd_7$ intermetallic phase (12.5%Ce, cubic a = 0.400 nm). We can therefore consider that the phases observed by XRD correspond to Ce–Pd solid solutions.

XRD diagrams in Fig. 5 were recorded after exposure of the reduced and passivated catalysts to air. In spite of this, the shift in the Pd(1 1 1) peak is clearly observable, thus indicating that the Ce–Pd alloy maintains stable after the passivation treatment. A similar behaviour has been observed in the case of Pt/CeO_2 and Pt/$(Ce,Tb)O_2$ catalysts reduced at temperatures ≥1173 K [6,20]. In this last case nanoparticles of a $PtCe_5$ intermetallic compound are formed that could be detected by both XRD and HREM on samples exposed to air after passivation. HREM images revealed the presence of a very thin protective CeO_2 overlayer encapsulating the intermetallic nanoparticles that very likely contributes to avoid the further reaction of the intermetallic compound with oxygen present in the air at room temperature. Such protective layer can form either by decoration of the intermetallic during the high temperature reduction step or by partial reoxidation of the intermetallic surface layers during the passivation step.

Fig. 6(a) shows a HREM image of the Pd(2.4 wt%)/CeO_2 catalyst reduced at 973 K in which a nanoparticle, of about 6 nm, is observed in top view. In the DDP of the image, Fig. 6(b), reflections of both CeO_2 and Pd along the [0 0 1] zone axis are observed as well as a series of Moiré reflections ($\mu_{-2,3}$, $\mu_{1,-1}$, $\mu_{-1,2}$, $\mu_{2,-2}$). Note that in this case the following orientation relationship between metal and support holds: (0 0 2)Pd||(0 0 2)CeO_2.

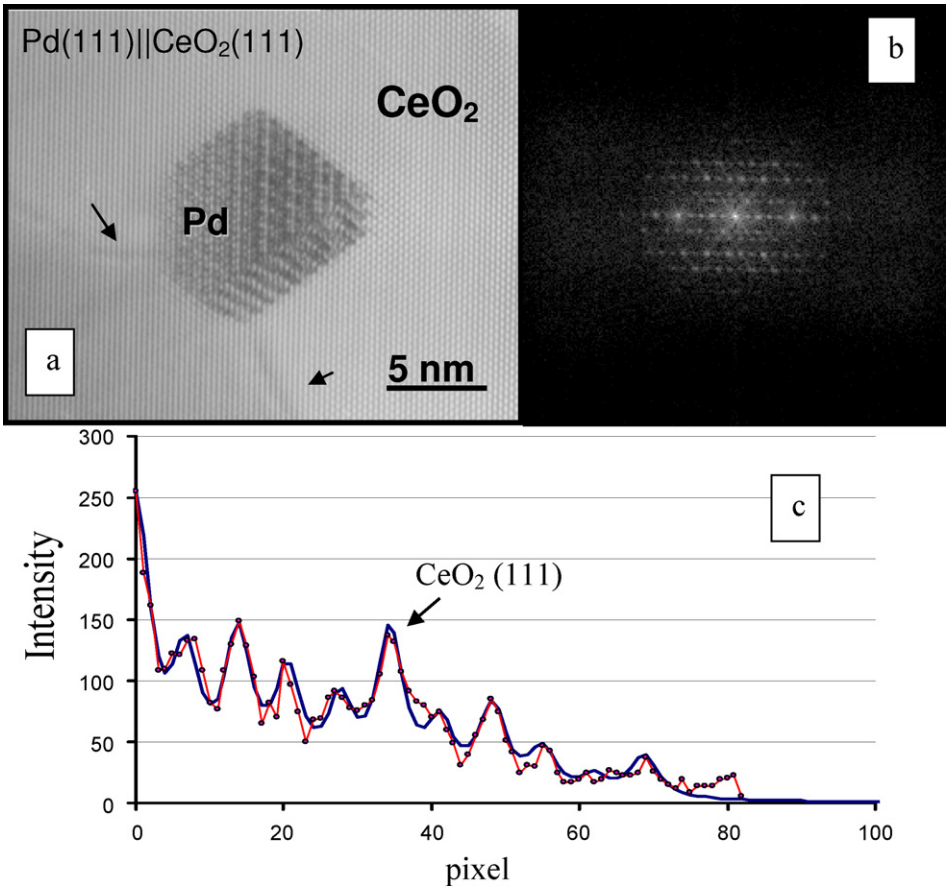

Fig. 7. (a) HREM image corresponding to the Pd(2.4 wt%)/CeO_2 sample reduced at 973 K. (b) DDP from (a). (c) Intensity profile from DDP.

The intensity profile along the ⟨1 0 0⟩ reciprocal direction of the DDP is shown in Fig. 6(c) (thin line with filled circles). The best fitting of the whole set of reflections included in this profile (thick line) was obtained for an expansion of the lattice parameter of palladium of +1.6 ± 0.2%, in very good agreement with the value estimated by XRD.

Data shown in Fig. 7 were also recorded on the catalyst reduced at 973 K and illustrate an interesting case. A twinned-type Pd particle is in this case observed in top view, Fig. 7(a). Both the metal and the support are imaged down the [1 1 0] zone axis. Note also the perfect alignment of both components, in a parallel indexes type orientation relationship. Thus the following relationships are clearly visible in the corresponding DDP, Fig. 7(b): $(1\,-1\,1)Pd||(1\,-1\,1)CeO_2$ and $(-1\,1\,1)\ Pd||(-1\,1\,1)CeO_2$. Fig. 7(c) depicts the intensity profile obtained along the ⟨1 −1 0⟩ reciprocal direction (thin line with filled circles). By applying the fitting procedure proposed herein, a contraction of −0.8 ± 0.2% could be determined. A quite good correlation between the position of the experimental Moirés and the fitted curve (thick line in Fig. 7(c)) is observed. This result, which was peculiar among the whole set of nanoparticles studied in our Pd/CeO_2 catalysts, can be rationalized if we think that the particle which is imaged in this case is embedded within the support. Reduction in hydrogen at 973 K leads to some sintering of the support. In fact after reduction at 623 K the BET surface area of the catalyst is 19 m^2/g and this value decreases down to 11 m^2/g after reduction at 973 K. If particles do not migrate on the surface during this process, the collapse of ceria crystallites may induce the occlusion of some nanoparticles which may eventually become stressed by the compression exerted by the surrounding support walls. Graham et al. [7] have reported the occurrence of Pd encapsulation in ceria-zirconia supported catalysts from the analysis of X-ray diffraction data.

Finally, Fig. 8 illustrates the analysis of the Pd(2.4 wt%)/CeO_2 catalysts after reduction at the highest temperature, 1173 K. The HREM image of Fig. 8(a) shows very clearly double diffraction effects. Fig. 8(b) shows the estimations of Pd(1 1 1) lattice spacing values using different reflections from the DDP of the particle. The average value obtained from these estimations indicated an expansion of Pd lattice of 2.0 ± 0.5%, in quite good agreement with XRD data.

The different examples commented on above illustrate that not only a precise value for the modification of the lattice parameter of nanoparticles can be obtained with our approach but also that the expansive/contractive nature of the modification can also be determined. Note also that the results obtained suggest that the high temperature reduction treatment involves the occurrence of both an alloy process between Ce and Pd and the loss of metal nanoparticles from the catalyst surface by ceria sintering-driven encapsulation. Both effects would certainly modify the chemical response of the catalyst.

3.3. *Application to Pd/CeO_2 catalysts reduced at low temperature*

The point we want to address now is how the procedure we have developed can be applied to systems containing smaller particles, in the range 2–5 nm. For this purpose we will investigate the nanostructure of a Pd(0.5 wt%)/CeO_2 catalyst reduced at low temperatures (623 K and 773 K).

Fig. 9 shows a general view of the Pd(0.5 wt%)/CeO_2 catalyst reduced at 623 K. Note how a large number of nanoparticles, with size in the 2–5 nm range, are observed, most of them in top view conditions. Most of the particles show low frequency, Moiré type,

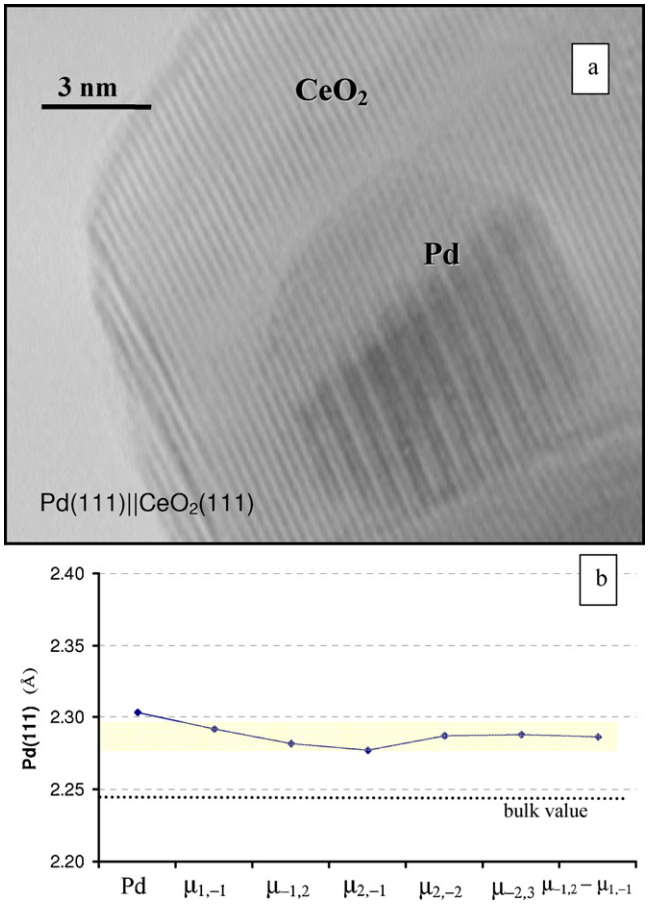

Fig. 8. (a) HREM image corresponding to the Pd(2.4 wt%)/CeO_2 sample reduced at 1173 K. (b) Pd(1 1 1) spacing values obtained from different Moiré reflections.

contrasts. The particles seem to be grown on different steps of a single CeO_2 crystallite. In fact the image shows contrasts which very clearly reveal the presence of these steps. It is also remarkable that the Moiré fringes observed in all the particles lay parallel to each other, all aligned along the same direction. This clearly indicates that the particles have grown under an orientation relationship onto the support, as previously described in the Pd(2.4 wt%)/CeO_2 catalyst. The contrasts indicate in fact a parallel orientation relationship between metal and support, which in this case can be described as (1 1 1)Pd||(1 1 1)CeO_2.

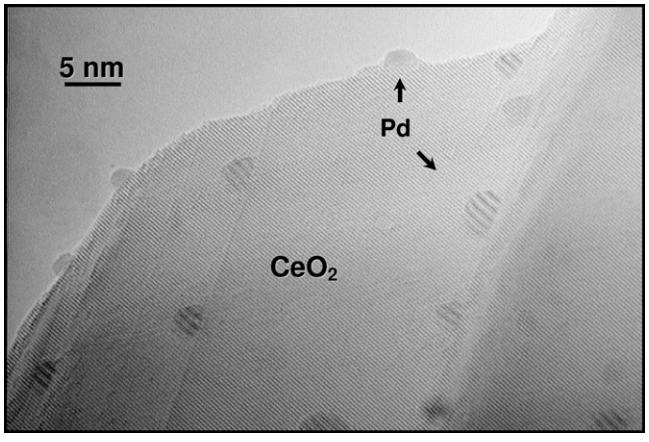

Fig. 9. HREM image from the Pd(0.5 wt%)/CeO_2 catalyst reduced in H_2/Ar flow at 623 K.

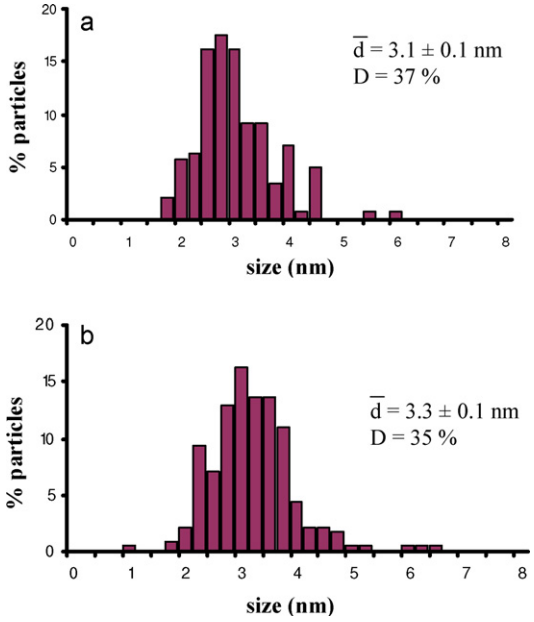

Fig. 10. Particle size distributions of the Pd(0.5 wt%)/CeO_2 catalyst reduced in H_2/Ar at (a) 623 K and (b) 773 K.

HREM images of the sample reduced at 773 K were similar, particles within the same size range and under the same orientation relationship with respect to the support were observed. In this case images showing both (1 1 1)Pd||(1 1 1)CeO_2 and (0 0 2)Pd||(0 0 2)CeO_2 orientation relationships were found.

Fig. 10 gathers the particle size distributions of the Pd(0.5 wt%)/CeO_2 catalyst reduced at the two temperatures. Note that the size-range, average particle size and metal particle dispersion of both samples are very close.

We applied the new procedure to estimate the lattice parameter to the HREM images of the Pd(0.5 wt%)/CeO_2 catalyst reduced at 623 K and 773 K. In this way, the number of analysed particles was large enough as to get statistically meaningful information.

Taking either CeO_2(1 1 1) or Ce(0 0 2) lattice spacing values as internal calibration, we have measured the values for the Pd lattice parameter in the two catalysts. Recalling that the lattice parameter of bulk Pd is $a = 0.38898$ nm [21] we have confirmed that many particles in the catalysts reduced at 623 K and 773 K deviate from this value. In general they show different expansion degrees with respect to the bulk. Maximum expansion values observed were around 6%.

This modification of the lattice parameter can be tentatively attributed to the structural match between the metal and the support. Regarding this idea, we could mention that 4 Pd(1 1 1) planes exactly match 3 CeO_2(1 1 1) planes with an expansion of only 4,2%. This type of structural coherence has been reported for Pd nanoparticles supported on MgO [22].

The formation of Pd β-hydrides can be ruled out as the cause of this expansion because, as already stated, the catalysts were evacuated in He at 773 K after reduction and at this temperature these hydrides decompose under inert atmosphere [23]. The incorporation of Ce into Pd can also be excluded since the onset of this process takes place at temperatures above 973 K.

Intrinsic size effects, associated to surface stress [24,25], can also be disregarded because these effects give rise in the case of metal nanoparticles of Pd and Ni to a contraction of the lattice parameter [25,26] which increases with decreasing particle size.

Table 3 shows the distribution, in percentages, of the expansion values for the two catalysts. From data in this Table it is evident that in both catalysts most particles are structurally tensioned and also

Table 3
Distribution of the expansion values.

Expansion (%)	Number of particles (%)	
	623 K	773 K
0–2	35	75
2–4	45	25
4–6	20	0

that increasing the reduction temperature from 623 K up to 773 K, tough it does not play a major influence on particle size, it changes dramatically the tension state of the nanoparticles. Increasing the reduction temperature from 623 K up to 773 K leads, according to our results, to an ensemble of particles in which the overall tension state has decreased. Note at this respect that the percentage of particles in which the expansion of the lattice parameter lies between 0 and 2% significantly increases in the sample reduced at 773 K and also that the maximum deviation of the lattice parameter is 4% in the catalyst reduced at the highest temperature.

Fig. 11 provides some data that allow us visualizing the influence of particle size on the values of the lattice expansion. In particular this figure plots the values of lattice expansion for a number of particles present in the low loading palladium catalyst vs particle size, in the 2–5 nm range. Dark symbols correspond to the catalyst reduced at 623 K whereas those light symbols are those of the sample reduced at 773 K. We note that in general, in good agreement with data in Table 3, the values of the catalyst reduced at lower temperature lie above those of the catalyst reduced at 773 K. Note however also that as the size increases the average expansion decreases changing from about 6% down to only 1% when going from 2.5 to 4 nm in the catalyst reduced at 623 K and from about 3% down to 1% in the catalyst reduced at 773 K.

In any case, the structural expansion encountered in this catalyst after reduction at low temperatures contrasts with the results found by XRD in the Pd(2.4 wt%)/CeO_2 catalyst. In that case the analysis of the Pd(1 1 1) peak indicated a negligible modification of the lattice parameter. To appreciate the potential of the HREM approach, it is worth commenting on this difference in more detail.

Fig. 12(a) shows the particle size distribution of the high loading Pd(2.4 wt%)/CeO_2 catalyst reduced at 623 K as determined by HREM. Note that in this case there is a large contribution of particles with size larger than 4 nm. In terms of number of particles this fraction represents about 40% of the total ensemble of nanoparticles. We should recall, however, that the contribution of any particle to XRD diagrams is not linearly related to its size. Instead, this contribution is weighted by the volume of the particles. Fig. 12(b) represents the cumulative volume of the Pd(2.4 wt%)/CeO_2 catalyst reduced at 623 K as a function of particle size (thick trace). Note how, as marked on the Figure, the fraction of particles with size below 5 nm, which according to our previous results show a measurable distortion of the lattice parameter, represents only 28% of the catalyst mass. Therefore the XRD diagram is dominated (72%) by the fraction of particles whose expected distortion would be close to zero. The volume averaged particle size obtained from the HREM particle size distribution is 7.2 nm which is quite close to the value determined from the analysis of the XRD Pd(1 1 1) peak (8 nm), so this is very likely why no deviation of the lattice parameter is detected from XRD measurements. The mass fraction of particles in the Pd(2.4 wt%)/CeO_2 catalyst that could present a deviation of lattice parameter represent a total loading of only about 0.5%, a value similar to that of the low loading catalyst we have investigated and whose XRD does not even evidence the presence of Pd peaks.

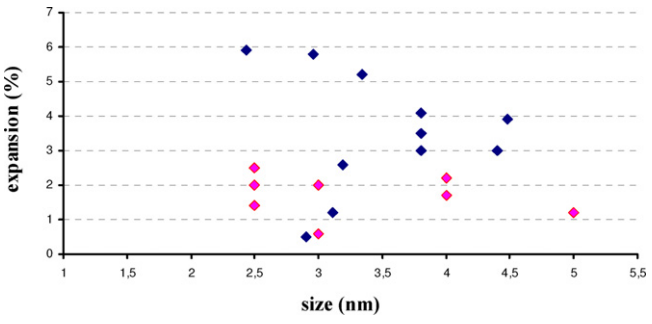

Fig. 11. Lattice expansion vs particle size of different Pd particles in the Pd(0.5 wt%)/CeO_2 catalyst reduced at 623 K (dark symbols) and 773 K (light symbols).

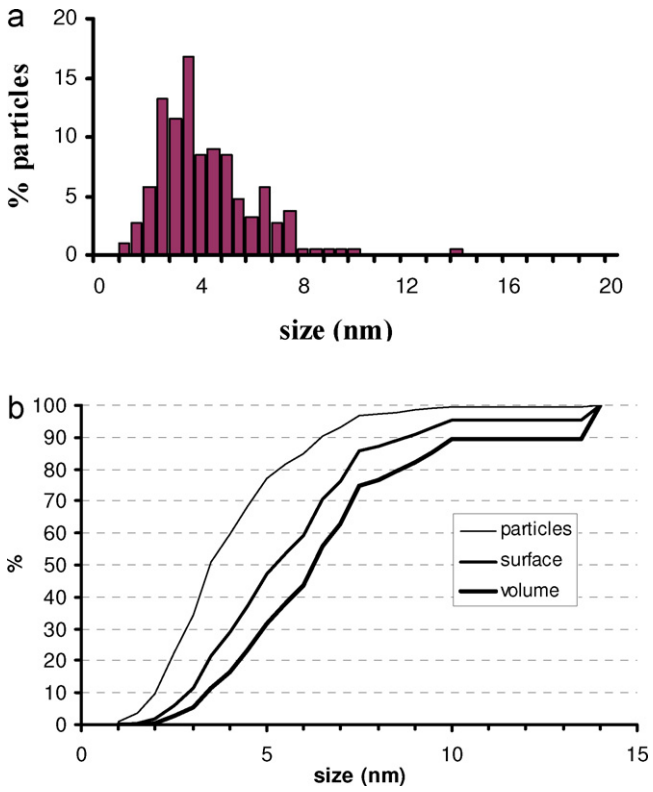

Fig. 12. (a) Particle size distribution of the Pd(2.4 wt%)/CeO_2 catalyst reduced in H_2/Ar at 623 K. (b) Cumulative fraction of particles, surface and volume in this sample.

Our results demonstrate however that this fraction of small particles in the high loading catalyst should present lattice parameters deviated from the bulk value if we admit, as it seems reasonable, a behaviour similar to that observed by HREM in the low loading one. If we take into consideration that these particles represent nearly 40% of the total surface exposed by Pd nanoparticles in the high loading catalyst, as marked on the cumulative plot of surface as a function of size plotted in Fig. 12(b), we conclude that they in fact represent a significant contribution to the catalytic and chemical behaviour of the system. In other words, nearly 40% of the Pd atoms exposed at the surface of the high loading catalyst reside on nanoparticles whose lattice parameter is slightly modified with respect to the bulk value whereas the remaining 60% is located onto particles with normal lattice parameter. This represents a 2/5 fraction of the total surface which is in our view an important question to take into account.

We should also highlight at this point that XRD cannot provide this detailed information regarding the fraction of particles with the smallest sizes (1–5 nm). In this case volume averaging and intrinsic size limits characteristic of this macroscopic technique put

emphasis on the information related to the larger particles present in the catalyst, this representing a serious limitation. The individual access to the information which provides HREM imaging is completely necessary to properly evaluate the exact structure of the system.

4. Conclusions

We have developed a new procedure to estimate the lattice spacing of supported nanoparticles based on the simultaneous analysis of single and double diffraction information contained in HREM images. The determination is based on the fitting of experimental intensity profiles recorded from DDP of top view HREM images with trial profiles generated by addition of Lorentzian functions centred at the position of Moirés estimated from a guess lattice parameter. A systematic search of the nanoparticle lattice parameter providing the best correlation between experimental and calculated profile is performed.

The accuracy of lattice particle determination on the basis of the use of Moiré reflections is analysed. In general our analysis indicates that, even by using a single Moiré, higher accuracies than that obtained on the basis of direct metal reflections are obtained. The accuracy can be improved if average values corresponding to estimations from different Moirés are calculated. Finally with the simultaneous, coupled, use of all the reflections in the DDP accuracy as high as 0.2% is possible.

The application of the more sophisticated fitting procedure to HREM images of nanoparticles observed in Pd/CeO_2 catalysts has allowed us to detect the very subtle modifications in the lattice parameter of the palladium nanoparticles induced by different reduction treatments. On the catalyst reduced at highest temperatures (>773 K), lattice expansions due to Ce–Pd alloying and lattice contractions related to nanoparticle occlusion within the support have been detected.

After reduction at low temperature (623–773 K), expansion of the lattice parameter of very small nanoparticles has been detected possibly motivated by a structural accommodation on the support crystallites. The expansion depends both on nanoparticle size and on the applied reduction temperature. Lower expansion values have been observed on the catalyst reduced at 773 K. Likewise the expansion decreases with particle size.

This procedure allows characterizing the lattice parameter of individual nanoparticles whose study is beyond the limits of XRD. The discussion made about the contribution to surface sites of the fraction of these particles not accessible by XRD has revealed the importance of performing the study of this aspect by means of HREM.

References

[1] A. Trovarelli, Catal. Rev. Sci. Eng. 38 (1996) 439.
[2] J. Kaspar, P. Fornasiero, M. Graziani, Catal. Today 50 (1999) 285.
[3] S. Bernal, J.J. Calvino, M.A. Cauqui, J.M. Gatica, C. Larese, J.A.P. Omil, J.M. Pintado, Catal. Today 50 (1999) 175.
[4] S. Bernal, G. Blanco, J.J. Calvino, J.M. Gatica, J.A. Pérez Omil, J.M. Pintado, Top. Catal. 28 (2004) 31.
[5] S. Bernal, F.J. Botana, J.J. Calvino, G.A. Cifredo, J.A. Pérez-Omil, J.M. Pintado, Catal. Today 23 (1995) 219.
[6] S. Bernal, J.J. Calvino, J.M. Gatica, C. Larese, C. López-Cartes, J.A. Pérez-Omil, J. Catal. 169 (1997) 510.
[7] G.W. Graham, H.-W. Jen, W. Chun, R.W. McCabe, Catal. Lett. 44 (1997) 185–187.
[8] L. Kepinski, M. Wolcyrz, Appl. Catal. 150 (1997) 197–220.
[9] S.-C.Y. Tsen, P.A. Crozier, J. Liu, Ultramicroscopy 98 (2003) 63–72.
[10] J.W.M. Jacobs, D. Schryvers, J. Catal. 103 (1987) 436–449.
[11] S. Giorgio, C.R. Henry, C. Chapon, J. Cryst. Growth 100 (1990) 254.
[12] C. Goyhenex, C.R. Henry, J. Urban, Philos. Mag. A 69 (6) (1994) 1073–1084.
[13] J.C. Jiang, X.Q. Pan, G.W. Graham, R.W. McCabe, J. Schwank, Catal. Lett. 53 (1998) 37–42.
[14] P.V. Menacherry, M. Fernandez-Garcia, G.L. Haller, J. Catal. 166 (1997) 75–88.
[15] C.T. Champ, W.A. Jesser, Ultramicroscopy 103 (2005) 165–172.
[16] J.-O. Malm, M.A. O'Keefe, Ultramicroscopy 68 (1997) 13–23.
[17] W.J. DE Ruijter, R. Sharma, M.R. McCartney, D.J. Smith, Ultramicroscopy 57 (1995) 409–422.
[18] S. Bernal, F.J. Botana, J.J. Calvino, C. López-Cartes, J.A. Pérez-Omil, J.M. Rodríguez-Izquierdo, Ultramicroscopy 72 (1998) 135–164.
[19] D. Rossi, R. Ferro, R. Marazza, J. Less Common Met. 40 (1975) 345–350.
[20] G. Blanco, J.J. Calvino, M.A. Cauqui, P. Corchado, C. López-Cartes, C. Colliex, J.A. Pérez-Omil, O. Stephan, Chem. Mater. 11 (12) (1999) 3610–3619.
[21] J. Waser, H.A. Levy, S.W. Peterson, Acta. Crystallogr. 6 (1953) 661.
[22] S. Giorgio, C.R. Henry, C. Chapon, C. Roucau, J. Catal. 148 (1994) 534–539.
[23] J.A. McCaulley, J. Phys. Chem. 97 (1993) 10372.
[24] D. Shreiber, W.A. Jesser, Surf. Sci. 600 (2006) 4584–4590.
[25] Z. Wei, T. Xia, J. Ma, W. Feng, J. Dai, Q. Wang, P. Yan, Mater. Charact. 58 (2007) 1019–1024.
[26] R. Lamber, S. Wetjen, N. Jaeger, Phys. Rev. B 51 (1995) 16.